Resolution Enhanced Distorted Born Iterative Method Using ROI Limiting Scheme for Microwave Breast Imaging

Yutaro Suzuki and Shouhei Kidera, *Senior Member, IEEE*

***Abstract*—This paper presents a high-resolution inverse scattering approach using the distorted Born iterative method (DBIM) by utilizing a region-of-interest limitation scheme that assumes microwave breast cancer imaging modality. The DBIM-based tomography approach provides a quantitative dielectric profile, contributing to reliable cancer recognition, especially for dense breast media. However, if the inversion cell is small, the original DBIM will be inaccurate because the unknowns will far exceed the number of data samples. Thus, high-resolution reconstruction is a challenging issue and is not unique only to the DBIM. To address this difficulty, this paper introduces a region-of-interest (ROI)-limited scheme by developing low-resolution DBIM images. Numerical tests based on 2D FDTD demonstrate that the proposed approach provides high-resolution and accurate dielectric profiles for highly heterogeneous realistic phantoms.**

***Index Terms*—Microwave imaging, contrast source inversion, multi-frequency integration, breast tumor imaging.**

I. Introduction

ACCORDING to global statistics, breast cancer is considered one of the most diagnosed and deadly cancers of all other malignant tumors. X-ray mammography, the most common screening technique for early-stage breast cancer, can result in harmful high-energy exposure to normal cells. It can also put high pressure on screening, which can reduce examination rates, especially for young women. Other low-pain, low-cost alternative modalities such as ultrasound imaging offer some advantages compared to X-ray screening. However, diagnosis performance depends on the experience of the operator. In this case, highly responsive fibroglandular tissues are often diagnosed as tumors, especially if the breast is dense. On the contrary, microwave-based imaging modality (*i.e.*, microwave mammography) has many benefits in terms of cost, safety, non-contact measurements, leading to more frequent screening and better recognition of early-stage cancer [1]–[3].

Many credible studies have shown significant contrast between normal and malignant tumor cells regarding permittivity and conductivity over the microwave frequency range [4]. Extraction of accurate dielectric profiles is directly related to higher recognition rates and is expected to reduce false-positive rates significantly. In the microwave imaging approach focused on breast cancer detection, radar imaging is one of the leading approaches, such as synthetic aperture [5], space-time beamforming [6], compressed sensing approaches [7], with the introduction of contrast agents such as magnetic nanoparticles. In particular, the multi-threshold-based iterative shrinkage algorithm was introduced in [8] for sparse regularization reconstruction in the compressed sensing scheme. However, it remains challenging to recognize cancerous tissue from highly scattered breast media. As another alternative imaging approach, the inverse scattering (tomography) methods have been intensively studied in recent years [9]–[12]. By solving the Helmholtz-type domain integral equation (DOI), the complex permittivity profile can be quantitatively obtained from several scattered fields recorded using arrays. There are two challenging issues with the inverse scattering problem. The first is non-linearity due to the multiple scattering effects caused by high contrast and heterogeneous media. This requires a solution to the nonlinear optimization problem using the forward solver. The other is an ill-posed feature, implying that the number of unknowns is considerably greater than the number of data samples. This ill-posedness can become more serious as the unknown grows, especially if sufficiently high-resolution images are required.

Following the above problem, this paper attempts to address with the second problem, that is, a resolution enhancement of the tomographic image. To achieve the above feature, we focus on the fact that the major part of breast media is dominated by low-contrast adipose tissue, the area of which can be eliminated from the region of interest (ROI). The proposed scheme is divided into two parts. The first process is a solution in low-resolution cells, and the entire breast, including adipose tissue, is considered ROI. The second step is to eliminate the adipose area from the ROI and run the solution in higher resolution cells using a lower reconstruction profile as the initial estimate. The inverse scattering approach employs the distorted Born iterative method (DBIM) proven in the literature [12]–[15]. Highly heterogeneous and high contrast media can be accurately reconstructed using a sequential optimization algorithm with forward and inverse solvers. Note that, in [16], the number of unknowns was reduced by employing the wavelet basis function in the DBIM scheme. In this scheme, an initial estimate of the DBIM reconstruction profile is used in the low-frequency data to obtain a more

Manuscript received August 29, 2021; accepted October 18, 2021. Date of publication November 2, 2021; date of current version November 22, 2021. This work was supported by MIC/SCOPE under Grant 162103102. *(Corresponding author: Shouhei Kidera.)*

The authors are with the Graduate School of Informatics and Engineering, University of Electro-Communications, Tokyo 1828585, Japan (e-mail: suzuki.yutarou@ems.cei.uec.ac.jp; kidera@uec.ac.jp).

Digital Object Identifier 10.1109/JERM.2021.3121962

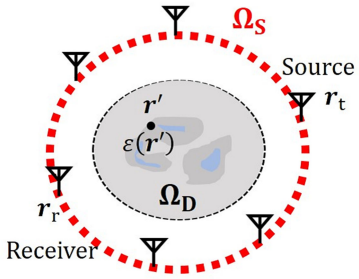

Fig. 1. Array and object configuration.

accurate reconstruction and not to enhance image resolution. In addition, in [17], high-resolution image conversions were proposed from the low-resolution reconstruction results, where five different background initial estimates can be processed in parallel. Although the approach adopted in this work is similar to the proposed method, it does not reduce the number of unknowns to alleviate an ill-posed condition. In contrast, the proposed scheme exploits not only a low-resolution image as an initial estimate for the high-resolution (HR) DBIM reconstruction, but also is capable of reducing the number of unknowns using a very straightforward approach. In this way, the adipose tissue cells can be eliminated from the ROI. Consequently, the proposed scheme exhibits the following two advantages, namely, a significant reduction of unknowns and an alleviation of the initial DBIM-scheme estimate dependency using low-resolution results. Using realistic MRI-derived phantoms, two-dimensional numerical tests show that our proposed method considerably enhances the accuracy of the reconstruction profile even at high-resolution imaging pixels and reduces the computational cost of high-resolution imaging.

II. Method

A. Observation Model

Fig. 1 shows an array and object configuration model. The breast media comprises adipose, skin, fibroglandular, and cancerous tissues with dispersive properties, modelled by a single-pole Debye model as in the literature [4]. The observation area, denoted by $\Omega_{\rm S}$ contains the breast with numerous transmitters and receivers, whose positions are defined as $\boldsymbol{r}_t$ and $\boldsymbol{r}_r$, respectively. The transmitted source current sequentially excites the electromagnetic wave radiation. This radiation illuminates an object and is recorded in the receiver as a total electric field defined as $E^{\rm T}(\boldsymbol{r}_t, \boldsymbol{r}_r; \omega)$ at the specific angular frequency ω.

B. Overview of Distorted Born Iterative Method (DBIM)

The DBIM is one of the most promising inverse solutions, which has been demonstrated even in highly heterogeneous and dispersive breast media [12]–[14]. A notable advantage of the DBIM is that it accurately reconstructs object functions with higher contrast by updating the background media. This can hardly be achieved by the first-order Born approximation. Let $E^{\rm I}(\boldsymbol{r}_t, \boldsymbol{r}_r; \omega)$ be the incident field at position $\boldsymbol{r}$ from the transmitter $\boldsymbol{r}_t$. Using the Helmholtz-type domain integral equation, the scattered field, $E^{\rm S}(\boldsymbol{r}_t, \boldsymbol{r}_r; \omega)$, is defined as follows:

$$\begin{aligned} E^{\rm S}(\boldsymbol{r}_t, \boldsymbol{r}_r; \omega) &\equiv E^{\rm T}(\boldsymbol{r}_t, \boldsymbol{r}_r; \omega) - E^{\rm I}(\boldsymbol{r}_t, \boldsymbol{r}_r; \omega) \\ &= k_{\rm b}^2 \int_{\Omega_D} G^{\rm B}(\boldsymbol{r}, \boldsymbol{r}'; \omega) E^{\rm T}(\boldsymbol{r}_t, \boldsymbol{r}'; \omega) \\ &\quad \times O(\boldsymbol{r}'; \omega) d\boldsymbol{r}', (\boldsymbol{r} \in \Omega_S), \end{aligned} \tag{1}$$

where $k_{\rm b}$ and $G^{\rm B}(\boldsymbol{r}, \boldsymbol{r}'; \omega)$ represent the wavenumber and Green's function of the background media, respectively. Ω_S and Ω_D are defined as the observation domain and the object domain, respectively, which are also known as the ROI. $E^{\rm T}(\boldsymbol{r}_t, \boldsymbol{r}_r; \omega)$ denotes the total field, whereas $O(\boldsymbol{r}; \omega) = (\epsilon(\boldsymbol{r}; \omega) - \epsilon_{\rm b}(\boldsymbol{r}; \omega))/\epsilon_{\rm b}(\boldsymbol{r}; \omega)$ represents the contrast function, where $\epsilon(\boldsymbol{r}; \omega)$ and $\epsilon_{\rm b}(\boldsymbol{r}; \omega)$ denote the complex permittivity of the object and background media at location $\boldsymbol{r}$, respectively. This paper defines $E^{\rm TB}(\boldsymbol{r}_t, \boldsymbol{r}_r; \omega)$ as the total field, assuming a specific background media. If $O(\boldsymbol{r}; \omega) \ll 1$ holds, then $E^{\rm T}(\boldsymbol{r}_t, \boldsymbol{r}'; \omega) \simeq E^{\rm TB}_{j,k}(\boldsymbol{r}'; \omega)$ also holds. That is, the first order Born approximation is well established. By introducing the variable $\Delta E^{\rm T}(\boldsymbol{r}_t, \boldsymbol{r}_r; \omega)$ defined as $\Delta E^{\rm T}(\boldsymbol{r}_t, \boldsymbol{r}_r; \omega) \equiv E^{\rm T}(\boldsymbol{r}_t, \boldsymbol{r}_r; \omega) - E^{\rm TB}(\boldsymbol{r}_t, \boldsymbol{r}_r; \omega)$, the following approximation is also well established:

$$\Delta E^{\rm T}(\boldsymbol{r}_t, \boldsymbol{r}_r; \omega) \simeq k_{\rm b}^2 \int_{\Omega_D} G^{\rm b}_j(\boldsymbol{r}, \boldsymbol{r}') E^{\rm TB}_{j,k}(\boldsymbol{r}'; \omega) O(\boldsymbol{r}'; \omega) d\boldsymbol{r}'. \tag{2}$$

The above description contains the fact that if we update the background media close to the actual object profile, the first order Born approximation will be applicable, even if the object profile has higher contrast than the initial background media. To obtain an accurate profile, the DBIM algorithm iteratively updates $\epsilon_{\rm b}(\boldsymbol{r}; \omega)$, $G^{\rm b}_j(\boldsymbol{r}, \boldsymbol{r}')$ and $E^{\rm TB}(\boldsymbol{r}_t, \boldsymbol{r}_r; \omega)$ to minimize $\sum_{\boldsymbol{r}_t, \boldsymbol{r}_r} |\Delta E^{\rm T}(\boldsymbol{r}_t, \boldsymbol{r}_r; \omega)|^2$.

C. Proposed Method

1) ROI Limitation Scheme: The DBIM and other inverse scattering approaches have the inherent problem of ill-posed conditions that can be fatal in high-resolution images due to the increased number of small cells that fill the entire ROI region. The literature [6], [18] indicates a strong need to achieve high-resolution dielectric profiles to achieve high-recognition rates, particularly in early malignancies. This paper introduces a two-step DBIM approach to address the above issue using the ROI limitation scheme and an appropriate initial estimate of background media.

The first step assumes a medium-resolution cell size with Δs. The DBIM reconstructs the dielectric profile of the entire breast, implying that the ROI is not limited. Here, the $\hat{O}(\boldsymbol{r}; \omega, \Delta s)$ is the contrast function reconstructed with low-resolution cells as:

$$\hat{O}(\boldsymbol{r}; \omega, \Delta s) = \mathcal{F}^{\rm DBIM}\left[E^{\rm S}(\boldsymbol{r}_t, \boldsymbol{r}_r; \omega); \Omega_D, \epsilon_{\rm b}(\boldsymbol{r}; \omega), \Delta s\right] \tag{3}$$

where $\mathcal{F}^{\rm DBIM}[E^{\rm S}(\boldsymbol{r}_t, \boldsymbol{r}_r; \omega); \Omega_D, \epsilon_{\rm b}(\boldsymbol{r}; \omega), \Delta s]$ denotes the conversion function from the scattered data $E^{\rm S}(\boldsymbol{r}_t, \boldsymbol{r}_r; \omega)$ to the

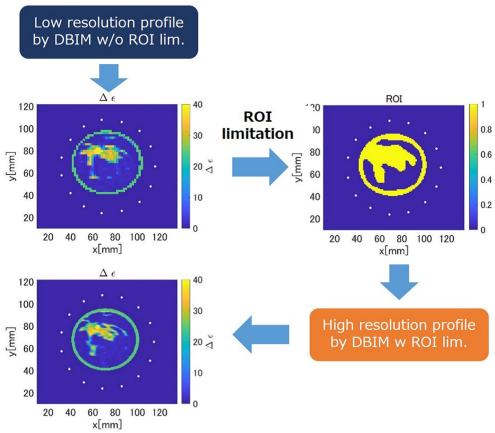

Fig. 2. Proposed scheme in converting low resolution profile to high resolution profile with ROI limitation.

contrast function $O(\boldsymbol{r};\omega,\Delta s)$ by the DBIM process described in Section II-B, assuming the background media $\epsilon_{\rm b}(\boldsymbol{r};\omega)$ and the ROI Ω_D with the cell size Δs. This process provides us a rough estimation of the complex profile with a certain level accuracy in assuming a relatively small number of unknowns.

2) CSI With Higher Resolution Cell: In the second step, an area with a low dielectric constant in $\hat{O}(\boldsymbol{r};\omega,\Delta s)$ is considered an adipose tissue, and is excluded from the ROI as follows:

$$\hat{\Omega}_D(\Delta s) \equiv \begin{cases} \Omega_D & (\hat{O}(\boldsymbol{r};\omega,\Delta s) \geq O_{\rm th}) \\ \varnothing & (\text{otherwise}) \end{cases} \tag{4}$$

where $\varnothing$ denotes the empty set, and $O_{\rm th}$ denotes the threshold of the contrast function. The dielectric profile of the area that is not considered as the ROI in Eq. (4) (namely, the background area) is replaced by that of an average adipose tissue denoted as $O_{\rm adi}$. The DBIM with high resolution cell $\Delta s/M$ uses the updated background $O(\boldsymbol{r};\omega,\Delta s)$ to resolve the following DIE as follows:

$$\hat{O}\left(\boldsymbol{r};\omega,\frac{\Delta s}{M}\right) = \mathcal{F}^{\rm DBIM}\left[E^{\rm S}(\boldsymbol{r}_t,\boldsymbol{r}_r;\omega);\hat{\Omega}_D(\Delta s),\hat{\epsilon}_{\rm b}(\boldsymbol{r};\omega,\Delta s),\frac{\Delta s}{M}\right], \tag{5}$$

where $\hat{\epsilon}_{\rm b}(\boldsymbol{r};\omega,\Delta s)$ is the complex permittivity of the background derived from $\hat{O}(\boldsymbol{r};\omega,\Delta s)$. Fig. 2 shows a schematic diagram of the proposed method. Note that, the proposed schemes offers not only an appropriately selected ROI (tissues with higher contrast), but also provides a good initial estimate of the background media by the contrast function $\hat{O}(\boldsymbol{r};\omega,\Delta s)$ with lower resolution cell, which enhances a computational efficiency and accuracy.

III. Numerical Simulation Results

A. Numerical Settings

In this section, a 2-D frequency-dependent FDTD-based numerical analysis is presented. The relevant code was first written by the Madison Cross-Disciplinary Electromagnetics Laboratory, University of Wisconsin, assuming a single-pole Debye model with a relaxation time of 15 ps. A realistic numerical phantom derived from MRI was used [19], where a matching media is set to air. In particular, a Class 3 (heterogeneously dense) phantom with a cross-section of $z = 64$ mm was envisioned, which is available in the literature [20]. The source current excited at each transmitter forms a raised-cosine modulated pulse with a center frequency of 2.45 GHz and a bandwidth of 2.7 GHz. There are 15 transmitters and receivers surrounding the breast media. A scattered electric field is measured at all combinations of them, which is 225. To validate the effectiveness of the proposed method, we assumed three resolution profiles: $\Delta s = 2$ mm, $\Delta s = 1$ mm, and $\Delta s = 0.5$ mm. Fig. 3 shows the original profile of Debye parameters $(\epsilon_\infty, \Delta\epsilon, \sigma_s)$ for Class 3 phantom resolution cell size. The unknowns are 728 for 2-mm cells, 2678 for 1-mm cells, and 10,735 for 0.5-mm cells, while the number of data samples is 1125 with five frequency samples (1.15 GHz, 1.84 GHz, 2.53 GHz, 3.22 GHz, and 3.91 GHz) and 225 observation patterns. In the DBIM updates, the l_2 norm regularization is introduced, and the regularization coefficient λ is set to 0.005.

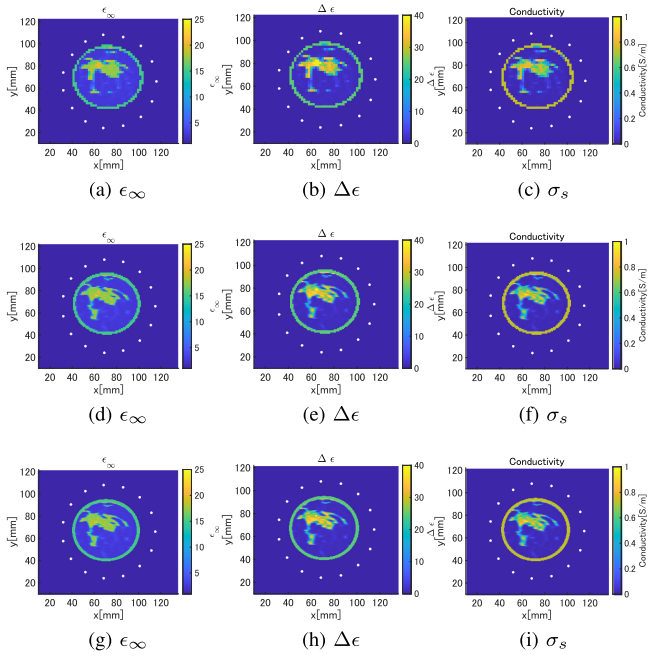

Fig. 3. Original profiles of Debye parameters in Class 3 with each cell size. (a)-(c): $\Delta s = 2$ mm. (d)-(f): $\Delta s = 1$ mm. (g)-(i): $\Delta s = 0.5$ mm.

B. Resolution Conversion Results

First, let us focus on the case with a cell resolution of 1 mm. Fig. 4 shows the reconstruction profiles obtained by the original DBIM, assuming $\Delta s = 1$ mm, which means that the entire breast media is set to ROI. For simplicity, we assumed a noise-free scenario to quantize the systematic error of each method. As shown in 4, the relatively high Debye parameter region, including cancerous tissue, can be reconstructed. However, the boundaries of skin, fibroglandular, and adipose are not well determined

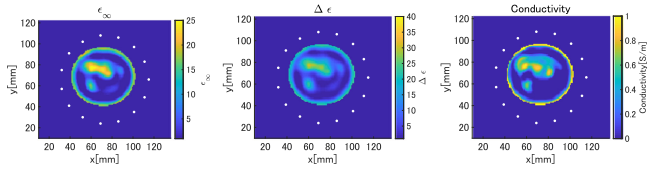

(a) ϵ_∞ (b) $\Delta\epsilon$ (c) σ_s

Fig. 4. Original DBIM with $\Delta s = 1.0$ mm.

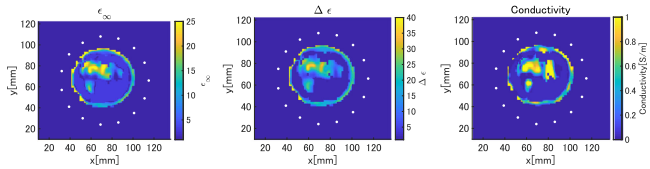

(a) ϵ_∞ (b) $\Delta\epsilon$ (c) σ_s

Fig. 5. Proposed DBIM from $\Delta s = 2$ mm to $\Delta s = 1$ mm.

TABLE I
DEBYE PARAMETERS USED IN THE PROPOSED METHOD FOR $O_{\rm th}$ AND $O_{\rm adi}$

	ϵ_∞	$\Delta\epsilon$	σ_s
$O_{\rm th}$	10	5.1	0.11
$O_{\rm adi}$	3.1	1.7	0.0367

compared to the original profile. In contrast, Fig. 5 shows the reconstruction results provided by the proposed method. Here, the Debye parameters of the threshold values $O_{\rm th}$ in Eq. (4)) and$O_{\rm adi}$ of the adipose tissue are summarized in Table I. In the original DBIM with $\Delta s = 2$ mm cell, $\hat{O}(\boldsymbol{r}; \omega, 2\tilde{}\mathrm{mm})$ was provided first, and the updated ROI $\hat{\Omega}_D(2\tilde{}\mathrm{mm})$ was processed sequentially in the DBIM with $\Delta s = 1$ mm cell using the initial estimate of background profile as $\hat{\epsilon}_{\rm b}(\boldsymbol{r}; \omega, 2\tilde{}\mathrm{mm})$. As shown in Fig. 5,the boundaries between tissues are more clearly recognized, and a more accurate profile is available by reducing the unknowns. Table II shows the quantitative comparison of the original and proposed DBIM methods in terms of the number of unknowns, computational time, and cumulative error probabilities that satisfy relative errors within 10 %. As shown in Table II, the proposed DBIM can offer not only more accurate reconstruction results of all Debye parameters, but also a lower computational cost than those obtained by the original DBIM, This is because the first step of the proposed DBIM is performed by low-resolution cells, reducing computational costs, especially if the FDTD-based forward solver is iteratively used with 2-mm cells. This is another advantage of the proposed method. Note that, the number of unknowns reduced by the proposed method slightly increases for a low SNR, because a low-resolution image is possibly contaminated by random noise and includes more unnecessary high-contrast cells.

Next, the 0.5-mm cell case is considered a higher resolution case. Fig. 6 shows the reconstruction profiles obtained by the original DBIM, assuming $\Delta s = 0.5$ mm. The reconstruction profiles also show that they cannot provide high contrast in regions containing fibroglandular or cancerous tissues. This is because the DBIM becomes inaccurate due to the extreme imbalance between the number of unknowns (10,735) and the number of

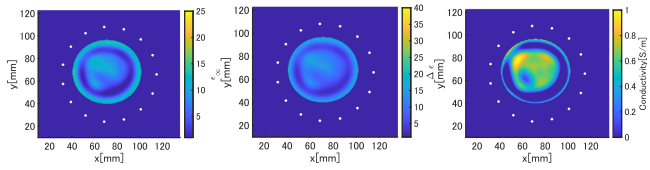

(a) ϵ_∞ (b) $\Delta\epsilon$ (c) σ_s

Fig. 6. Original DBIM with $\Delta s = 0.5$ mm.

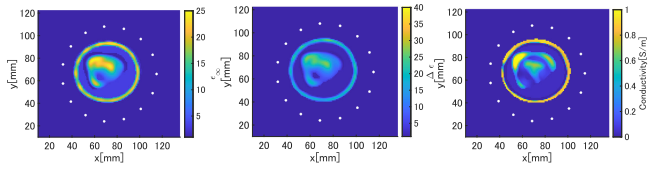

(a) ϵ_∞ (b) $\Delta\epsilon$ (c) σ_s

Fig. 7. Proposed DBIM from $\Delta s = 1$ mm to $\Delta s = 0.5$ mm.

data samples (1125). This imbalance may cause a local optimum problem. Fig. 7 shows the reconstruction profiles based on the proposed method. Here, the original DBIM with $\Delta s = 1$ mm cell was computed as $\hat{O}(\boldsymbol{r}; \omega, 1\tilde{}\mathrm{mm})$ and the DBIM with $\Delta s = 0.5$ mm cell was computed with the updated ROI $\hat{\Omega}_D(1\tilde{}\mathrm{mm})$ using the initial background profile as $\hat{\epsilon}_{\rm b}(\boldsymbol{r}; \omega, 1\tilde{}\mathrm{mm})$. As shown in Fig. 7, even in extremely ill-conditioned cases, high contrast regions, fibrous tissues, and cancerous tissues can be accurately reconstructed. This is because the proposed method initially employs the reconstruction result of 1 mm namely, the better conditioned case. Table III summarizes the comparison of quantitative performance similar to Table II. As shown in Table III, the proposed method maintains the same cumulative probability level within a relative error of 10 % compared to the 1-mm case, even in very high-resolution scenarios with short computational times. In visual term, the accuracy conductivity profile may be relatively worse than the other Debye parameters shown in Figs. 5 or 7. However, the quantitative analysis presented in Tables II and III clearly demonstrates the efficiency of the proposed method, particularly for the $\Delta s = 1$ mm $\rightarrow 0.5$ mm case. Furthermore, in the proposed method, the contrast function corresponds to the average number of adipose tissues $O_{\rm adi}$ defined in Eq. (4), that is, assuming homogeneity in the outside of the ROI. In contrast, since an original property of adipose tissue depends on a cell position, naturally, the assumed homogeneous profile with $O_{\rm adi}$ in the proposed method would not exactly express the original profile in the adipose area. Therefore, the improvement in the cumulative probabilities shown in Tables II and III is derived not only from the adipose, but also from the fibro-glandular or cancer area.

C. Sensitivity to Noise

Finally, the noise robustness of the proposed method is examined as follows. Similar to related literature [21], [22], white Gaussian noise was added to the scattered electric field. The signal-to-noise ratio (SNR) is defined as the ratio of the maximum power of the received signal to the average noise power in the time domain. Fig. 8 shows the reconstruction profiles of the

TABLE II
CUMULATIVE PROBABILITIES SATISFYING WITHIN 10 % RELATIVE ERROR (2 MM → 1 MM)

	Number of unknowns	Computation time	ϵ_∞	$\Delta\epsilon$	σ_s
Original DBIM	2678	8500 s	15.5%	23.7%	43.5%
Proposed DBIM	728 → 1460	4690 s	47.1%	44.6%	47.0%

TABLE III
CUMULATIVE PROBABILITIES SATISFYING WITHIN 10 % RELATIVE ERROR (1 MM → 0.5 MM)

	Number of unknowns	Computation time	ϵ_∞	$\Delta\epsilon$	σ_s
Original DBIM	10735	118613 s	12.5%	1.46%	27.7%
Proposed DBIM	2678 → 6848	53460 s	38.1%	34.8%	44.1%

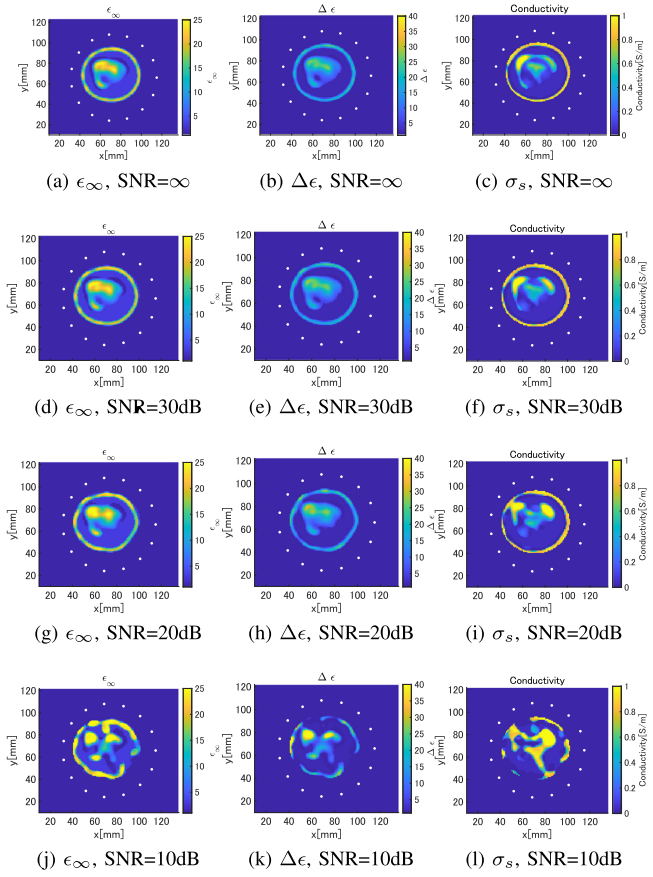

(a) ϵ_∞, SNR=∞ (b) $\Delta\epsilon$, SNR=∞ (c) σ_s, SNR=∞
(d) ϵ_∞, SNR=30dB (e) $\Delta\epsilon$, SNR=30dB (f) σ_s, SNR=30dB
(g) ϵ_∞, SNR=20dB (h) $\Delta\epsilon$, SNR=20dB (i) σ_s, SNR=20dB
(j) ϵ_∞, SNR=10dB (k) $\Delta\epsilon$, SNR=10dB (l) σ_s, SNR=10dB

Fig. 8. Reconstruction results of the proposed method from $\Delta s = 1$ mm to $\Delta s = 0.5$ mm.

TABLE IV
CUMULATIVE PROBABILITY SATISFYING WITHIN 10% RELATIVE ERROR (1 MM → 0.5 MM) IN EACH SNR LEVEL

SNR	Number of unknowns	ϵ_∞	$\Delta\epsilon$	σ_s
∞	6848	38.1%	34.8%	44.1%
30 dB	6864	38.9%	35.8%	44.8%
20 dB	6782	40.1%	37.0%	45.7%
10 dB	6966	32.0%	33.1%	39.5%

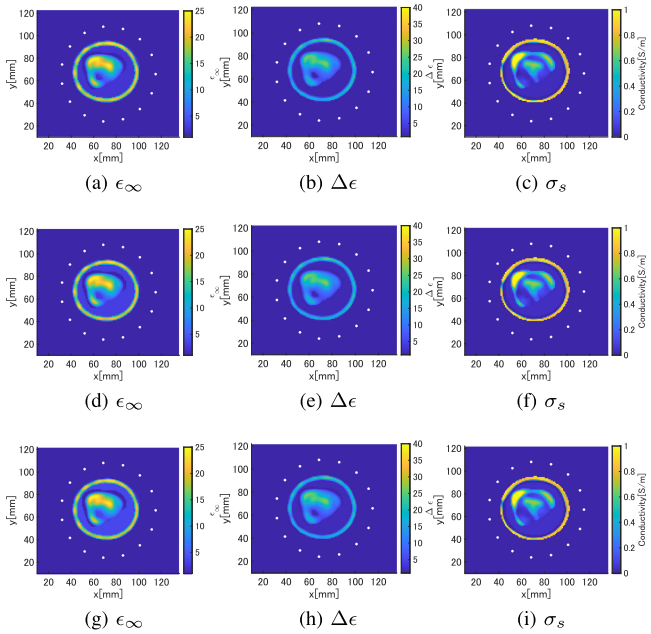

(a) ϵ_∞ (b) $\Delta\epsilon$ (c) σ_s
(d) ϵ_∞ (e) $\Delta\epsilon$ (f) σ_s
(g) ϵ_∞ (h) $\Delta\epsilon$ (i) σ_s

Fig. 9. Reconstruction results (1 mm → 0.5 mm) in varying the value of $O_{\rm adi}$. First and second denote the cases when $O_{\rm adi}$ are set as $0.8 \cdot O_{\rm adi}^{\rm orig}$ and $1.2 \cdot O_{\rm adi}^{\rm orig}$, respectively.

proposed method, which assumes conversion from 1-mm cells to 0.5-mm cells at each level of SNR. Table IV shows a quantitative error analysis that introduces the cumulative probability with a relative error of less than 10 %. These figures and tables clearly demonstrate that the proposed method has a certain level of noise robustness beyond 20 dB SNR cases. On the other hand, at 10 dB SNR, the reconstruction profile is distorted due to the random noise effect.

D. Sensitivity to Selected Parameters

A sensitivity analysis with respect to the $O_{\rm th}$ and $O_{\rm adi}$ parameters was conducted to validate the robustness of the proposed method. Here, we focus on the $O_{\rm adi}$ parameter since this parameter directly affects the reconstruction results produced by the proposed method. These results are presented in Fig. 9 shows the reconstruction results in "1 mm → 0.5 mm" cases, where the selected adipose tissues were varied from their original values $O_{\rm adi}^{\rm orig} = (3.1, 1.7, 0.0367)$ shown in Table I. The sensitivity to $O_{\rm adi}$ was assessed by investigating the $O_{\rm adi} = 1.2 \cdot O_{\rm adi}^{\rm orig}$ and $O_{\rm adi} = 0.8 \cdot O_{\rm adi}^{\rm orig}$ values. The cumulative probabilities considering the error criteria is presented in Table V. The results show

TABLE V
CUMULATIVE PROBABILITY SATISFYING WITHIN 10% RELATIVE ERROR (1 MM → 0.5 MM) IN VARYING O_{adi}

O_{adi}	ϵ_∞	$\Delta\epsilon$	σ_s
$0.8 \cdot O_{\mathrm{adi}}^{\mathrm{orig}}$	36.1 %	34.4 %	44.0 %
$1.0 \cdot O_{\mathrm{adi}}^{\mathrm{orig}}$	38.1 %	34.8 %	44.1 %
$1.2 \cdot O_{\mathrm{adi}}^{\mathrm{orig}}$	24.2 %	14.2 %	44.1 %

no significant sensitivity with respect to O_{adi}. This is because the accuracy enhancement of the reconstruction is dominant in the limited ROI area, *i.e.*, the region that includes the fibro-glandular or cancer tissues. Note that, the cumulative probabilities of ϵ_∞ and $\Delta\epsilon$ are downgraded only for the $O_{\mathrm{adi}} = 1.2 \cdot O_{\mathrm{adi}}^{\mathrm{orig}}$ value in compared with σ_s, which remains stable. However, the advantage from the original DBIM is still, maintained, as shown in Table III.

Next, the effect of the l_2-norm regularization coefficient in the DBIM is discussed. In the DBIM method, the l_2-norm regularization is used to update the objective function, where its coefficient λ is fixed to 0.005 for all cases. This value was empirically adjusted in [15]. It is predicted that by selecting the value of λ, the reconstruction result can be affected in any resolution case, and the proper selection of λpossibly improves the performance. However, the optimization of λ for each resolution level is generally difficult. In contrast, the number-of-unknowns reduction scheme is effective since an ill-posed condition can be alleviated by the ROI limitation even in selecting any λ. This has already been demonstrated in the results shown in Figs. 6 and 7. It is observed that the reconstruction results are further improved, even when using the same regularization coefficient $\lambda = 0.005$.

IV. CONCLUSION

We focus on the DBIM based complex permittivity profile reconstruction assuming microwave breast cancer imaging. The inherent problem in the inverse scattering analysis, namely, an ill-conditioned problem, can be significantly alleviated by introducing low-resolution cell initial estimates and ROI limiting schemes. Two-dimensional FDTD numerical analysis assumes a very heterogeneous and realistic breast phantom. The proposed method has succeeded in improving the resolution of the reconstructed profile with high accuracy, especially in high contrast tissue regions. In addition, the proposed method has a computational cost advantage over the original DBIM by introducing a low-resolution reconstruction step. Note that, although the smallest wavelength assumed even in the highest contrast breast tissues was larger than 1.0 mm, the 0.5-mm cell inversion, which was demonstrated in [17], is meaningful. This is because the reconstruction accuracy of the CSI is determined by the discretization level when calculating the domain integration in Eq.(1), and it is the same when calculating the forward problem using the FDTD, where an $1/10$ smaller wavelength is selected to achieve accurate results. The present study has addressed the 3D extension and experimental validations. The effectiveness of this approach becomes even more apparent in 3D problems where the unknowns increase significantly. In addition, the radar-based ROI limitation scheme [23] is a promising method for achieving more accurate reconstruction, and it will be investigated in a future work.

REFERENCES

[1] P. M. Meaney, M. W. Fanning, D. Li, S. P. Poplack, and K. D. Paulsen, "A clinical prototype for active microwave imaging of the breast," *IEEE Trans. Microw. Theory Techn.*, vol. 48, no. 11, pp. 1841–1853, Nov. 2000.

[2] E. C. Fear, J. Bourqui, C. Curtis, D. Mew, B. Docktor, and C. Romano, "Microwave breast imaging with a monostatic radar-based system: A study of application to patients," *IEEE Trans. Microw. Theory Techn.*, vol. 61, no. 5, pp. 2119–2128, May 2013.

[3] E. Porter, M. Coates, and M. Popovic, "An early clinical study of time-domain microwave radar for breast health monitoring," *IEEE Trans. Biomed. Eng.*, vol. 63, no. 3, pp. 530–539, Mar. 2016.

[4] M. Lazebnik *et al.*, "A large-scale study of the ultrawideband microwave dielectric properties of normal, benign, and malignant breast tissues obtained from cancer surgeries," *Phys. Med. Biol.*, vol. 52, pp. 6093–6115, 2007.

[5] H. Song *et al.*, "Detectability of breast tumors in excised breast tissues of total mastectomy by IR-UWB-Radar-Based breast cancer detector," *IEEE Trans. Biomed. Eng.*, vol. 66, no. 8, pp. 2296–2305, Aug. 2019.

[6] E. J. Bond, Xu S. C. Li Hagness, and B. D. V. Veen, "Microwave imaging via space-time beamforming for early detection of breast cancer," *IEEE Trans.: Antennas Propag.*, vol. 1, no. 8, pp. 1690–1705, Aug. 2003.

[7] M. T. Bevacqua and R. Scapaticci, "A compressive sensing approach for 3D breast cancer microwave imaging with magnetic nanoparticles as contrast agent," *IEEE Trans. Med. Imag.*, vol. 35, no. 2, pp. 665–673, Feb. 2016.

[8] M. Ambrosanio, P. Kosmas, and V. Pascazio, "A multi-threshold iterative DBIM-based algorithm for the imaging of heterogeneous breast tissues," *IEEE Trans. Biomed Eng*. vol. 66, no. 2, pp. 509–520, Feb. 2019.

[9] P. M. Meaney, S. D. Geimer, and K. D. Paulsen, "Two-step inversion with a logarithmic transformation for microwave breast imaging," *Med. Phys.*, vol. 44, no. 8, pp. 4239–4251, Aug. 2017.

[10] J. D. Shea, B. D. V. Veen, and S. C. Hagness, "A TSVD analysis of microwave inverse scattering for breast imaging," *IEEE Trans Biomed Eng.*, vol. 59, no. 4, pp. 936–945, Apr. 2012.

[11] H. Sato and S. Kidera, "Noise-robust microwave breast imaging applied to multi-frequency contrast source inversion," *IEEE J. Electromagn., RF, Microw. Med. Biol.*, vol. 5, no. 2, pp. 187–193, Jun. 2021.

[12] D. W. Winters, B. D. V. Veen, and S. C. Hagness, "A sparsity regularization approach to the electromagnetic inverse scattering problem," *IEEE Trans. Antennas Propag.*, vol. 58, no. 1, pp. 145–154, Jan. 2010.

[13] F. Gao, Barry D. V. Veen, and S. C. Hagness, "Sensitivity of the distorted born iterative method to the initial guess in microwave breast imaging," *IEEE Trans. Antennas Propag.*, vol. 63, no. 8, pp. 3540–3547, Aug. 2015.

[14] L. M. Neira, B. D. V. Veen, and S. C. Hagness, "High-resolution microwave breast imaging using a 3-D inverse scattering algorithm with a variable-strength spatial prior constraint," *IEEE Trans. Antennas Propag.*, vol. 65, no. 11, pp. 6002–6014, Nov. 2017.

[15] K. Noritake and S. Kidera, " Boundary extraction enhanced distorted born iterative method for microwave mammography," *IEEE Antennas Wireless Propag. Lett..*, vol. 18, no. 4, pp. 776–780, Apr. 2019.

[16] R. Scapaticci, P. Kosmas, and L. Crocco, "Wavelet-based regularization for robust microwave imaging in medical applications," *IEEE Trans. Biomed. Eng.*, vol. 62, no. 4, pp. 1195–1202, Apr. 2015.

[17] Z. Miao and P. Kosmas, "Multiple-frequency DBIM-TwIST algorithm for microwave breast imaging," *IEEE Trans. Antennas Propag.*, vol. 65, no. 5, pp. 2507–2516, May 2017.

[18] M. Mehranpour *et al.*, "Robust breast cancer imaging based on a hybrid artifact suppression method for early-stage tumor detection," *IEEE Access*, vol. 8, pp. 206790–206805, 2020, doi: 10.1109/ACCESS.2020.3037450.

[19] M. J. Burfeindt *et al.*, "MRI-derived 3D-printed breast phantom for microwave breast imaging validation," *IEEE Antennas Wireless Propag. Lett.*, vol. 11, pp. 1610–1613, 2012, doi: 10.1109/LAWP.2012.2236293.

[20] "Numerical breast phantom repository," [Online]. Available: https://uwcem.ece.wisc.edu/phantomRepository.html

[21] C. Gilmore, A. Abubakar, W. Hu, T. M. Habashy, and P. M. van den Berg, "Microwave biomedical data inversion using the finite-difference contrast source inversion method," *IEEE Trans. Antennas Propag.*, vol. 57, no. 5, pp. 1528–1538, May 2009.
[22] J. D. Shea, P. Kosmas, B. D. V. Veen, and S. C. Hagness, "Contrast-enhanced microwave imaging of breast tumors: A computational study using 3-D realistic numerical phantoms," *Inverse Problems*, vol. 26, no. 7, Jul. 2010, Art. no. 074009.
[23] A. Baran, D. J. Kurrant, A. Zakaria, E. C. Fear, and J. LoVetri, "Breast imaging using microwave tomography with radar-based tissue-regions estimation," *Prog. Electromagn. Res.*, vol. 149, pp. 161–171, 2014.

Yutaro Suzuki received the B.E. degree from the Faculty of Informatics and Communication Engineering, University of Electro-Communications, Tokyo, Japan, in 2020.

Shouhei Kidera (Senior Member, IEEE) received the B.E. degree in electrical and electronic engineering, and the M.I. and Ph.D. degrees in informatics from Kyoto University, Kyoto, Japan, in 2003, 2005, and 2007, respectively. Since 2009, he has been with the Graduate School of Informatics and Engineering, University of Electro-Communications, Tokyo, Japan, and is currently an Associate Professor. He has been stayed with the Cross-Disciplinary Electromagnetics Laboratory, University of Wisconsin-Madison, Madison, WI, USA, as a Visiting Researcher in 2016. He has been a Principal Investigator of the PRESTO Program of Japan Science and Technology Agency (JST) from 2017 to 2021. His research interests focuses on advanced radar signal processing or electromagnetic inverse scattering issue for ultrawideband (UWB) three-dimensional sensor or bio-medical applications. He was the recipient of the 2012 Ando Incentive Prize for the Study of Electronics, 2013 Young Scientist's Prize by the Japanese Minister of Education, Culture, Sports, Science and Technology (MEXT), and 2014 Funai Achievement Award. He is a Member of the Institute of Electronics, Information, and Communication Engineers of Japan (IEICE), Institute of Electrical Engineering of Japan (IEEJ), and Japan Society of Applied Physics (JSAP).